Chemical Geology 440 (2016) 42–49

Contents lists available at ScienceDirect

Chemical Geology

journal homepage: www.elsevier.com/locate/chemgeo

Review article

Simulation of geochemical banding I: Acidization-precipitation experiments in a ferruginous limestone rock

Maysam Msharrafieh, Mazen Al-Ghoul, Farah Zaknoun, Houssam El-Rassy, Samia El-Joubeily, Rabih Sultan *

Department of Chemistry, American University of Beirut, Beirut, Lebanon

ARTICLE INFO

Article history:
Received 31 March 2016
Received in revised form 28 June 2016
Accepted 29 June 2016
Available online 2 July 2016

Keywords:
Liesegang
Geochemical self-organization
Acidization
Banding in rocks

ABSTRACT

This paper is the first among two articles which aim at exploring the possible similarities between the well-known Liesegang banding phenomenon in precipitate systems, and the stripe formation observed in a large number of rocks. In the present (first) article, we review a comprehensive and long study wherein patterning experiments were performed in-situ (real rock systems), to simulate the band formation through the acidization of a ferruginous limestone rock, causing dissolution and precipitation reactions. The results are analyzed by microscopy, AA and XRD techniques. The correlation between the Liesegang gel experiment and the processes taking place inside the rock medium is established. In the second part (following paper), a theoretical model is set forth to support our experiments. The fractal nature of the contours of the various regions will be explored.
© 2016 Elsevier B.V. All rights reserved.

Contents

1. Introduction . . . 42
1.1. Rock acidization . . . 43
1.2. The study . . . 44
1.3. Similarities with systems in other Science fields - universality . . . 44
2. Acid-infiltration experiments . . . 44
2.1. Setup . . . 44
2.2. Preliminary tests . . . 45
2.3. Composition analysis of the treated rock . . . 45
3. Results and discussion . . . 45
3.1. Stage I: zonation in a short-span infiltration experiment . . . 45
3.2. X-ray analysis . . . 47
3.3. Stage II - long-span experiment . . . 47
4. Conclusions . . . 48
Acknowledgements . . . 48
References . . . 49

1. Introduction

The similarity between Liesegang bands observed in the laboratory, and geochemical self-organization has struck a wide group of scientists and stimulated research to unravel possibly common mechanistic scenarios. In this paper, we shed light on such similarities between the band formation in rocks (Fig. 1a) and the well-known Liesegang banding phenomenon (Liesegang, 1896; Hedges, 1932; Henisch, 1988). Liesegang precipitation bands are obtained when co-precipitate ions interdiffuse in a gel medium due to a cycle of supersaturation, nucleation and depletion (Ostwald, 1896–1902), coupled to the on-going diffusion process. Beautiful bands of precipitate appear as a result of this complex physico-chemical scenario. In various Liesegang patterns, spatial oscillations are displayed as periodic bands of precipitate in 1D, rings in 2D and shells in 3D, separated by precipitate free domains. A panorama of Liesegang bands involving several sparingly soluble salts is depicted in Fig. 1b.

* Corresponding author.
E-mail address: rsultan@aub.edu.lb (R. Sultan).

http://dx.doi.org/10.1016/j.chemgeo.2016.06.028
0009-2541/© 2016 Elsevier B.V. All rights reserved.

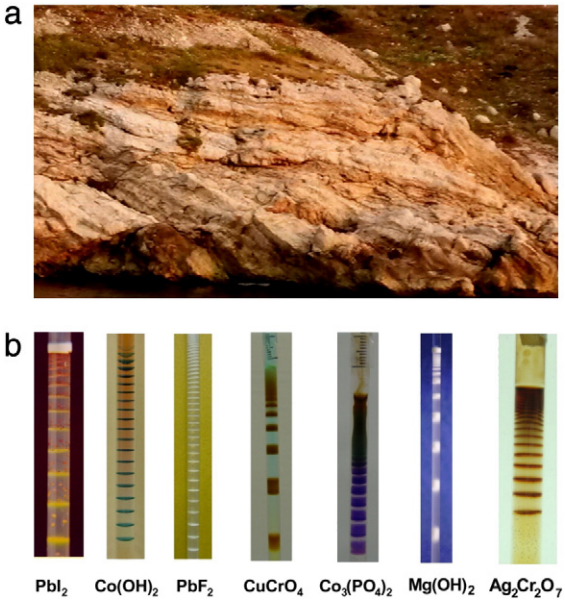

Fig. 1. a. A calcarous rock with stripes of hematite near the coast of Marseille-France. b. Liesegang "ringorama" for a variety of sparingly soluble salt systems, displaying colorful patterns of parallel bands.

Analogies with the Liesegang phenomenon in stones and rocks include parallel bands of minerals, concentric rings, oscillatory periodic zoning, stylolites, agates, geodes, concretions, orbicules and some other patterns. Many types of rocks display patterned textures with periodic banding, which might involve a Liesegang type of scenario. Examples include, to name but a few, banded iron oxide minerals, zebra spar (Krug et al., 1994), wood-grained chert and periodic oscillatory zoning (Ortoleva, 1994). Banded agates and geodes (Moxon, 1996, 2001) are often cited as typical paradigms of Liesegang structures in Geology. Hematite rings in sandstones constitute a close example of rhythmic banding similar to a Liesegang type experiment. A comprehensive survey of studies where the analogy between Liesegang bands and geochemical banding is unravelled, was conducted and presented in Sadek and Sultan (2011).

Stripes of iron oxide minerals deposit behind an oxidative water front infiltrating a rock bed hosting pyrite (FeS_2), as the main mineral. The acidic water causes the dissolution of pyrite, releasing Fe^{2+}, which is in turn oxidized, provoking the banded deposition of goethite [Fe(III)O(OH)] behind the pyrite dissolution front. A mechanism for this scenario of band formation was simulated (Sultan et al., 1990), and conjectured based on a bifurcation of the Ostwald supersaturation-nucleation-depletion cycle (Ostwald, 1896–1902).

Ring-shaped aggregates of hematite (cherry red Fe_2O_3) on the scale of several tens of microns, and rhyolite [totally alkali silica (TAS) SiO_2] on a millimeter scale, often garnish the texture of some commonly observed rocks (Ohkawa et al., 2000). The latter one is referred to as the Liesegang stone (displayed later in Fig. 4a). Banding in sphalerite was shown (Fowler and L'Heureux, 1996) to arise from an alternation of zinc and iron contents in an oscillatory mechanism, under from far-from-equilibrium crystallization conditions. Fine-scale layering ranging from mm to cm length scales develop in certain igneous intrusions (Boudreau, 1995), during in-situ crystallization processes. Such layered structures of the norite mineral are observed in rocks from the Stillwater Complex (Montana, USA), displaying even inch-scale "doublet" layers (Boudreau, 1995), just like in complex Liesegang systems. Using a cellular automaton model, Böhm et al. (2003) conjectured complex ryhthmicities of marl-limestone alternations, with striking resemblance to multiple-precipitate Liesegang patterns displaying strange periodicity, prepared in the laboratory (Msharrafieh and Sultan, 2005).

Although the mechanism of formation of agates might be different from a Liesegang scenario, they are typically and inevitably associated with an analogy to Liesegang bands in Geochemistry. Agates consist of microcrystalline SiO_2 tight aggregates, exhibiting a rich alternation of colored stripes, attributed to the impurities present in the SiO_2 matrix. A wide variety of microcrystalline silica polymorphs such as chalcedony, carnelian, amethyst, jasper, opal, and flint appear as layers which are deposited from aqueous solutions (Klein, 1993). The formation of the moss agate can be simulated by precipitating iron (II) silicate solution in water glass, in a way analogous to the reaction-diffusion processes within the magma causing the growth of ring-shaped domains in the agate rock upon cooling of the melt (http://onezine.s-one.net.sg/@School/RI/garden.htm).

Band formation in geochemical systems may involve a wide variety of scenarios. The stacking of banded deposits in aged rocks by mere sedimentation is not considered a self-organization phenomenon (Merino and Wang, 2001). We focus on systems that are believed to have generated banded patterns due to a nonequilibrium instability inherent in the dynamical processes that couple within the rock medium. A number of comprehensive studies, notably involving theoretical modeling have demonstrated a Liesegang-type mechanistic scenario, from the intrinsic nonlinear dynamics of the rock system. Such mechanisms were notably emphasized in the work by Ortoleva (1994), Ortoleva et al. (1987a, 1987b), Merino and Wang (2001), Wang et al. (2015), Wang and Merino (1992), Boudreau (1995, 1997), Fowler and L'Heureux (1996), L'Heureux (2013), and Chacron and L'Heureux (1999) groups. There is still debate as to the mechanism of Liesegang band formation itself. The proposed models fall into two main categories: pre-nucleation models based on the Ostwald supersaturation-nucleation-depletion models (Ostwald, 1896–1902); and post-nucleation theories based on the instability break-up of a uniform precipitate sol, mediated by Ostwald ripening (Ostwald, 1900; Ratke and Vorhees, 2002) and the Lifshitz-Slyozov instability (Lifshitz et al., 1961).

In the present paper (Part I), we review the entire experimental work performed on acidization-precipitation experiments in-situ, presented at a number of conferences (Msharrafieh et al., 2006; Sultan and Abdel-Rahman, 2011, 2013; Zaknoun et al., 2010). In a subsequent paper (Part II), we present a theoretical model (incorporating the visions of both schools) to simulate our experimental results, and carry out a fractal analysis of the contours of the various banded regions.

1.1. Rock acidization

Banded rock formations often arise from the cyclic precipitation as mineral-rich water infiltrates a porous rock and reacts to form an insoluble product (Ortoleva, 1994). This occurs through the coupling of the precipitation reaction with diffusion and percolation.

Extensive experiments and studies on rock acidization were conducted in dolomite (Lund et al., 1973), and sandstone cores (Lund and Fogler, 1976), though without attention to pattern formation. In this paper, we review an experiment carried out in-situ, wherein an acid is allowed to slowly infiltrate through a rock medium by means of a regulated infusion pump. We treat a sample of limestone rock, rich in calcite mineral ($CaCO_3$). A flow of acidic water causes the dissolution of calcite according to the following equation:

$$CaCO_3(s) + 2H^+(aq) \rightarrow Ca^{2+}(aq) + CO_2(g) + H_2O(l) \quad (1)$$

The presence of SO_4^{2-} anions (from sulfuric acid H_2SO_4) in the infiltrating stream can precipitate anhydrite ($CaSO_4$) or gypsum ($CaSO_4 \cdot 2H_2O$), according to the reaction:

$$Ca^{2+}(aq) + SO_4^{2-}(aq) \rightarrow CaSO_4(s) \quad (2)$$

An illustration of the geological scene with such operative scheme is depicted in Fig. 2.

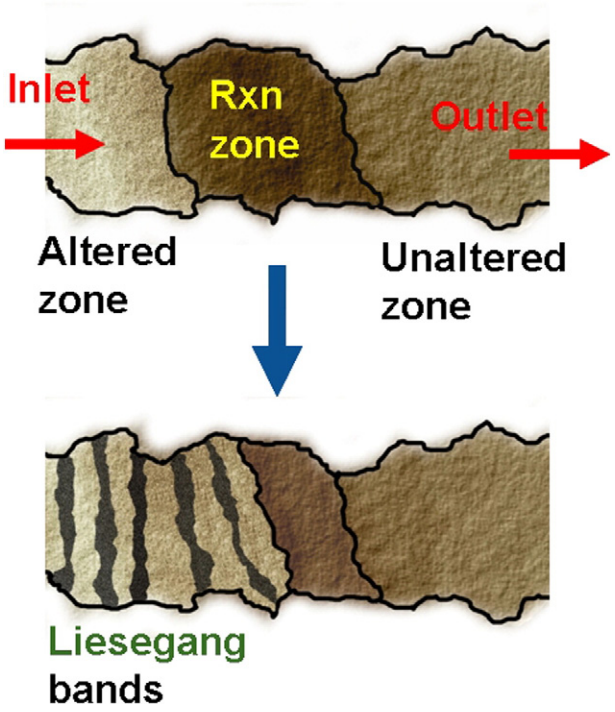

Fig. 2. An illustration of the imagined scenario believed to operate in our acidization experiments. UP: Reactive Acidic water (H^+) infiltrated through a porous limestone rock ($CaCO_3$), causing its dissolution generating Ca^{2+} and CO_2 (Reaction 1). DOWN: Banded deposition (Liesegang bands) of gypsum ($CaSO_4 \cdot 2H_2O$) or anhydrite ($CaSO_4$) behind the above dissolution front (Reaction 2).

1.2. The study

Most simulations of geochemical self-organization in the literature are limited to Liesegang-type experiments in gels, not in real rocks. The Liesegang gel method was used to model gallstone formation in vitro, in an attempt to simulate the conditions and processes underlying the deposition of bile salt systems (Peng et al., 1997; Xie et al., 1999). In the first part (Part I) of this study, we review previous acidization-precipitation experiments performed in-situ, using porous ferruginous limestone rock samples. In a following paper (Part II), we present a reaction-transport model to initiate a theoretical study, that will serve as a basis for unraveling the mechanistic properties of the observed acidization-precipitation phenomena. A fractal analysis of the contour morphologies of the precipitate deposit regions will also be carried out. Note here that theoretical studies for the simulation of geochemical self-organization are widely found in the literature (Sultan et al., 1990; Kruhl, 1994; Dewers and Ortoleva, 1989).

We investigate the phenomenon of band formation in rocks by simulating one possible scenario that would take place in a real, rock medium. Instead of focusing on the study of existing, "ready made" banded patterns in rock specimens, we force and steer the band deposition inside a rock bed, by simulating the physico-chemical processes which lead to such deposition, thus exactly mimicking the real natural scenario. This is done by infiltrating a ferruginous limestone rock with sulfuric acid, causing the dissolution of the bare rock calcite ($CaCO_3$) medium (Reaction 1), followed by the deposition of anhydrite ($CaSO_4$) or gypsum ($CaSO_4 \cdot 2H_2O$), behind the dissolution front (Reaction 2).

Thus, we carry out our experiments in-situ, spanning long times as required by the appearance of the desired patterns. To our knowledge, no investigator adopted this approach to geochemical self-organization before. The study would rather routinely be based on the analysis of existing rock specimens displaying parallel bands, or essentially, on theoretical modeling and numerical simulations. The mechanism involves diffusion and percolation of the infiltrating solution, coupled to chemical reactions driving dissolution, porosity changes and precipitation. The mineral deposition requires a collective scenario of nucleation, as well as competitive growth of both nuclei and larger particles of precipitate. A representative schematic picture of the dynamical events is illustrated (in reduced form) in the following scheme, and portrayed in Fig. 3:

$$A(s) + 2X(aq) \rightarrow Y(aq) \quad (3)$$

$$X(aq) + Z(aq) \rightarrow B(s) \quad (4)$$

where A represents a solid mineral (here calcite, $CaCO_3$), Y the dissolved salt material (Ca^{2+}), from the reaction with X (acidic water, H^+), Z the counter-ion from the infiltrating solution (here SO_4^{2-}) which reacts with Y to form precipitate B ($CaSO_4$).

Thus, this scheme (also illustrated in Fig. 3) is a simplified form of chemical reactions 1 and 2.

1.3. Similarities with systems in other Science fields - universality

Liesegang systems share a great deal of similarity with natural systems displaying striped patterns and ripple morphology, notably in Biology and Geology. Biological rhythmic patterns are manifest in the stripes on tigers and zebras, belts of bacteria colonies (Shapiro and Dworkin, 1997; Kravchenko et al., 1999), gallstones (Peng et al., 1997; Xie et al., 1999) and cysts. In Geology, agates and banded rocks present a typical example of rhythmic patterns (Ortoleva, 1994; Moxon, 1996, 2001; Ohkawa et al., 2000; Fowler and L'Heureux, 1996; Kruhl, 1994; Liesegang et al., 1913; Jamtveit and Meakin, 1999), and are perhaps the closest widespread natural phenomenon to the Liesegang stratification, because they directly involve precipitation and mineral deposition. Pictorial specimens of periodic banding in real natural geological systems are displayed in Fig. 4.

Between the rapid growth of bacterial colonies and the tremendously slow formation of rock patterns, we realize that self-organization can take place on a huge range of time scales (minutes to millions of years). A comprehensive review of the many similarities existing between Liesegang banding and paradigms of parallel stripe formation in Biology, Chemistry, Physics, Geology, Engineering and Medicine is presented in Sadek and Sultan (2011).

2. Acid-infiltration experiments

2.1. Setup

A sample of red brown, porous ferruginous limestone rock was infiltrated by a 4.0 M H_2SO_4 solution by means of an infusion pump (Thermo-Orion M361 Multi-rate Infusion Pump). The acid was delivered through a Tygon tube (3 mm in diameter), inserted in a tiny orifice

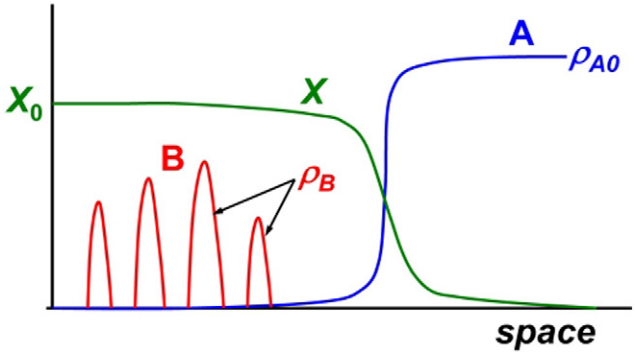

Fig. 3. Moving dissolution front of mineral A, infiltrated by aqueous species X, and producing the banded deposition of mineral B, upon reaction of Y with Z.

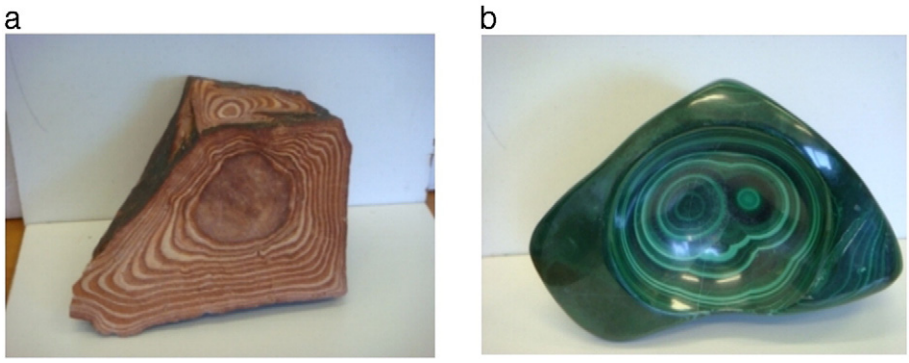

Fig. 4. Patterns of bands in natural stone systems (geology). a. Liesegang stone: a highly silicated banded rhyolite, a typical felsic volcanic rock; b. an agate of malachite, hydrous copper carbonate. Width of the rhyolite specimen is 10 cm and that of the malachite specimen is 12 cm.

carefully drilled at the center of the rock sample, 1.0 cm in depth. The delivery rate was regulated by the special pump at 1.0 mL per hour. With this injection setup from a large reservoir, a well-controlled flow could be attained. A schematic representation of the experimental setup is depicted in Fig. 5.

2.2. Preliminary tests

A number of simple preliminary chemical tests were first carried out to guide our analysis, while the final rock composition in various band domains is confirmed by X-ray analysis.

1. A zone rich in $CaCO_3$ is indicated by an effervescence upon treatment with 6 M HCl, due to the reaction:

$$CaCO_3(s) + 2HCl(aq) \rightarrow Ca^{2+}(aq) + 2Cl^{-}(aq) + CO_2(g) + H_2O(l) \quad (5)$$

2. A zone consisting of predominantly $CaSO_4$ would show no fizzing (effervescence) upon treatment with HCl.
3. An inter-band zone void of $CaSO_4$ showing no reaction upon addition of HCl is an indication of the depletion of the bare rock medium of any carbonate, due to prior consumption by the originally infiltrating acid (H_2SO_4). This would leave only the other minerals supporting the bare rock medium.
4. A small sample of white salt from a $CaSO_4$ ring partially dissolved in HCl, yields a yellow solution, attributed to the presence of ferric ions originating from the rock medium (ferruginous limestone). The presence of Fe^{3+} is confirmed by testing with KSCN solution. Upon addition of a few drops of SCN^{-}, the solution turned blood-red indicating the formation of the $Fe(SCN)^{2+}$ complex.
5. Flame atomic absorption analysis of the precipitate (done on a Thermo-elemental Solaar atomic absorption spectrophotometer), in $CaSO_4$-rich regions (after partial dissolution in HCl) was carried out to determine the elemental mass ratio of Calcium to Iron (Msharrafieh et al., 2006).

2.3. Composition analysis of the treated rock

The treatment was fulfilled in a series of experiments, the latest of which was extended over a period of about one year and eight months. In the latter (most recent) experiment, the H_2SO_4 infusion was kept on for 692 days. The final pattern was examined to delineate the various regions wherein $CaSO_4$ bands may have formed. The pattern span area was divided into eight main textural regions, as highlighted in Fig. 6. The delineation between the various regions was based on a visual color contrast, observed distinctly between the successive belt zones originating from the center (see notably Fig. 13, at 202 and 673 days).

Powder samples from each region were taken and placed in small tubes, which were stoppered thereafter. Each sample was analyzed by powder X-ray diffraction. Each diffractogram was mapped onto a Library of standard diffractograms for the calcite, gypsum and anhydrite minerals. After the peaks for each mineral were identified, the relative mass proportions of each mineral in the sample mixtures were determined by integrating the area under the bands of each mineral (Suryanarayana and Grant Norton, 1998). The average composition of every region in each of the three minerals (over a representative number of samples) could then be calculated.

3. Results and discussion

3.1. Stage I: zonation in a short-span infiltration experiment

At a first stage, the analysis of a treated ferruginous limestone rock was performed in a preliminary experiment wherein the H_2SO_4 infiltration was stopped at time $t = 161$ days. Texture and color modifications were monitored to delineate the various regions where the various

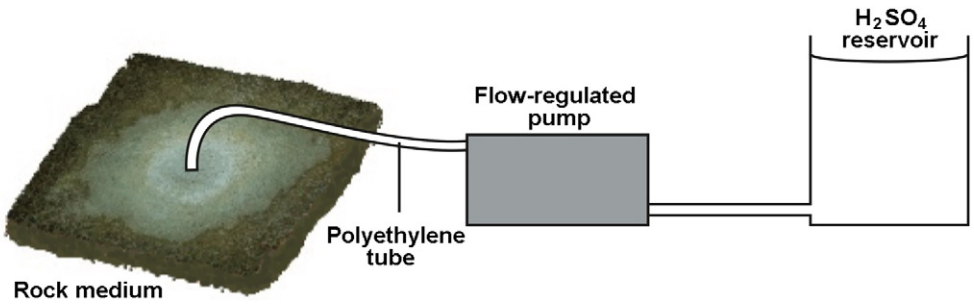

Fig. 5. Experimental setup: the pump regulates the flow of acid which subsequently infiltrates the rock.

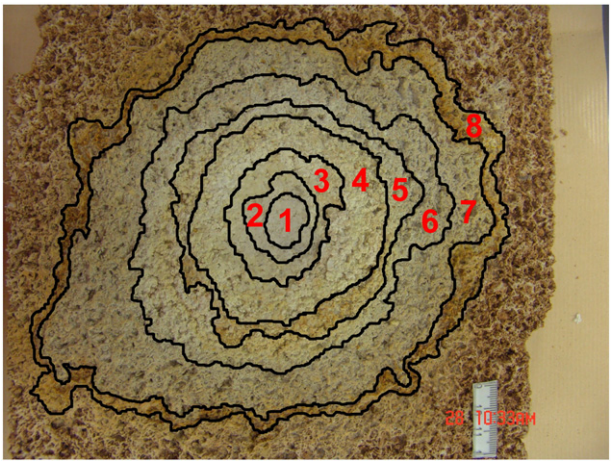

Fig. 6. Final rock pattern at $t = 692$ days. The rock was partitioned into eight "banded" zones for differentiation by X-ray analysis.

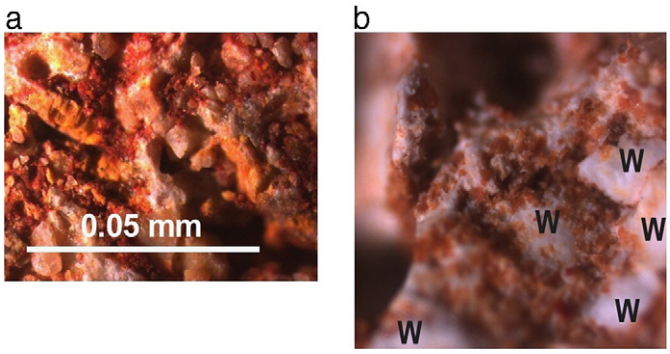

Fig. 8. Rock texture before (a) and after (b) acid injection. The latter displays the white crystals of $CaSO_4$ (labeled W) embedded within the rock. The two photomicrographs are of the same magnification (10×). The scale is indicated on the picture.

chemical changes had taken place. After 161 days of steady acid injection (4.0 M H_2SO_4), the rock had the appearance shown in Fig. 7.

The precipitation starts immediately after the acidization dissolution, through the formation of a heavy white deposit concentrated in a circular zone surrounding the injection center (Fig. 7). The precipitate is primarily confirmed to be $CaSO_4$, as no effervescence is produced by treatment with 6 M HCl, which indicates the depletion of the central region in carbonates by virtue of Reaction 5. $CaSO_4$ will later be confirmed by X-ray. Beyond this zone, the bare rock prevails (but $CaCO_3$-free because of acidization), followed by a belt of white precipitate, thus displaying an alternation of $CaSO_4$ and $CaSO_4$-free domains, just like in a Liesegang-type experiment. It would be certainly hasty to generalize that the overall mechanism is a Liesegang mechanism. We note however that this observation at the early stage of the pattern formation points toward that evidence, notably the presence of a zone void of $CaSO_4$ in the interband region. To compare the $CaCO_3$-rich bare rock with the $CaSO_4$-deposit region, photomicrographs of the two zones are depicted in Fig. 8. Frame a shows the bare rock before the reaction, while the acidized-deposited medium is seen in frame b. The white crystals, labeled " W" (frame b), consisting of the salt $CaSO_4$, are distinctly seen to be embedded within the rock after the dissolution and precipitation reactions 5 and 2. We now examine the belt region under the microscope.

A photomicrograph of the white ring zone was taken with a Nikon (COOLPIX 4500) digital camera, through the lens of a fluorescence microscope (Zeiss AXIOVERT 200). The rock texture in that domain is depicted in Fig. 9. The interface between the white precipitate and brown region (below it) indicates the position of the acidization front. The red arrows point to the tail of the precipitate belt.

For a preliminary description of the chemical alterations within the rock, we carried out simple tests as described in Section 2.2. When the white salt from both the central region and the white ring were treated with HCl, no effervescence was observed, confirming the absence of carbonate and hinting toward the prevalence of $CaSO_4$ as the main product from Reaction 2. The bare rock medium manifested excessive effervescence due to its richness in $CaCO_3$. The presence of Fe^{3+} in the rock medium (ferruginous limestone) was confirmed by testing with KSCN solution (after dissolving a small sample in HCl). Upon addition of a few drops of SCN^-, the solution turned blood-red indicating the formation of the $FeSCN^{2+}$ complex. Flame atomic absorption analysis of the precipitate (done on a Thermo-elemental Solaar atomic absorption spectrophotometer), in both the ring and the central region was then undertaken to determine the elemental mass ratio of calcium to iron. The results are recorded in Table 1.

The central region is much richer in calcium ions (compared with Fe^{3+}) confirming that the obtained precipitate is overwhelmingly calcium sulfate. In the ring domain, both iron and calcium are present in an

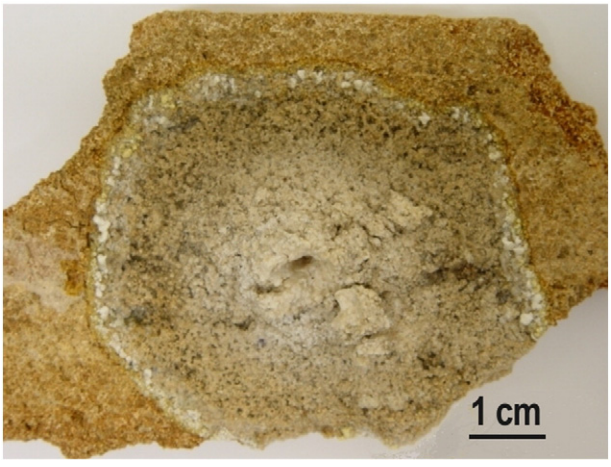

Fig. 7. $CaSO_4$ deposition in the limestone rock sample, infiltrated by H_2SO_4. The central region is a dense precipitate zone. Then, beyond a brown depleted zone, a distinct belt of $CaSO_4$ suggests the formation of a first Liesegang ring. The photo is taken on day 161. A 1 cm scale is indicated on the picture.

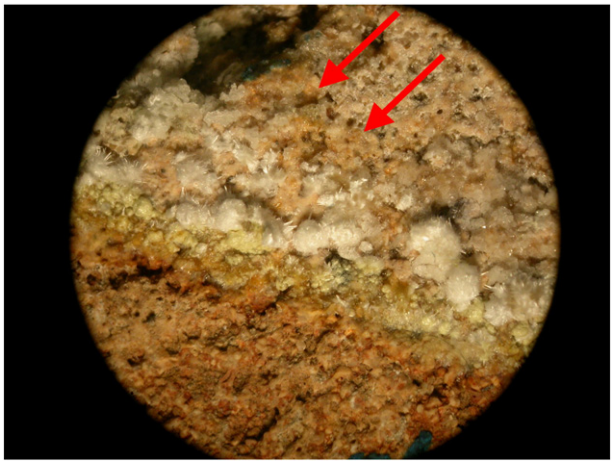

Fig. 9. Photomicrograph showing the texture contrast between the bare rock (lower portion) and the acid-invaded zone (upper portion), demarcated by the white and slightly yellow crystals (at the center). The picture is obtained at a 4× optical zoom magnification. The diameter of the displayed rock portion is approximately 1.5 cm. The red arrows indicate the position of the front, moving downwards.

Table 1
Analysis of the ring domain for Ca and Fe obtained by flame atomic absorption analysis. The second and third columns indicate the concentrations in mg/L (ppm) of Fe and Ca. These concentrations are converted to masses, and the mass ratio of calcium to iron is finally calculated (last column).

Sample ID	Fe (ppm)	Ca (ppm)	m_{Fe} (mg)	m_{Ca} (mg)	m_{Ca}/m_{Fe}
Center	3.528	36.19	0.0353	0.3620	10.3
Ring	9.629	8.947	0.09626	0.08947	1.08

Table 2
Relative abundance of $CaSO_4$ and $CaCO_3$ in the central region, the remote ring (1st Liesegang band) and the bare rock. The presence of $CaSO_4$ in the ring is confirmed.

	Bare rock	Central region	Ring
Total counts (gypsum + anhydrite)	36.4	742.8	279.3
Total counts of calcite	569	35.8	114.9
Ratio $CaSO_4/CaCO_3$	0.0640	20.7	2.43

almost 1:1 ratio. For a rigorous characterization of the various domains in the treated rock, we carried out an X-ray crystallographic analysis.

3.2. X-ray analysis

Powder X-ray diffraction data were collected using the reflection geometry. The X-ray diffractometer (Bruker D8 Discover) was run at 40 kV and 40 mA. The steps are in increments of 0.01°, and counts were collected at 0.5 s per step. Low angles (large *d*-spacings) lie to the left. The X-ray diffractogram for the bare rock is highlighted in Fig. 10. It clearly shows the dominance of the calcite ($CaCO_3$) mineral, with only very few traces of gypsum. This is also confirmed in the counts recorded in Table 2.

The analysis of the white precipitate in the central region, shown in Fig. 11, reveals that it is predominantly gypsum, and to a lesser extent, anhydrite. Traces of monohydrocalcite ($CaCO_3 \cdot H_2O$) were also identified (two low intensity peaks at $2\theta = 36.2°$ and 51.5°). Note that the calcite, anhydrite and gypsum peaks (C, A and G respectively) all lie in the region between $2\theta = 20°$ and 60°. Table 2 shows that in the central region, $CaSO_4$ (gypsum or anhydrite) is overwhelmingly dominant over $CaCO_3$. The latter mineral had essentially dissolved by virtue of Reaction 1.

Finally, the presence of $CaSO_4$ in the ring is confirmed as demonstrated in Fig. 12. Table 2 shows that gypsum is dominant over calcite. This realization is the most important result in this first stage of the study, as it reveals to a great extent the viability of a Liesegang-type scenario in certain pattern forming processes in rocks.

3.3. Stage II - long-span experiment

Another longer experiment was carried out at a second stage, spanning one year and eight months. The rock pattern appearance at various stages of the infiltration process is depicted in Fig. 13.

The experiment was described in Section 2.1, and the analysis procedure was presented in Section 2.3. Samples from each of the regions shown in Fig. 5 were taken by drilling small holes in different spots of the desired zone, then collecting the powder in small vials. The diffractograms confirmed the formation of gypsum ($CaSO_4 \cdot 2H_2O$), which was quite dominant over anhydrite ($CaSO_4$, anhydrous) as the main deposit product in Reaction 2. The central region (domains 1, 2 and 3) consists almost entirely of gypsum. Then depletion starts in region 4 (like in a real Liesegang pattern wherein bands start separating from a uniform zone that extends over a relatively wide spatial

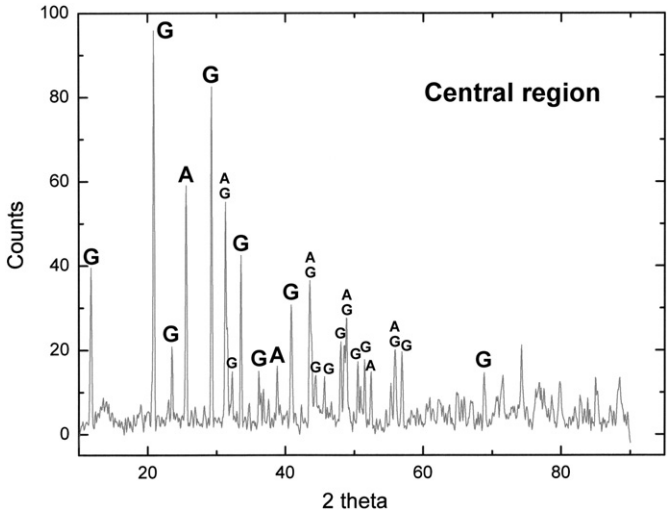

Fig. 11. Powder X-ray diffractogram of the central region where excessive precipitation has taken place. The peaks labeled A (anhydrite) and G (gypsum) reveal that the region is exclusively $CaSO_4$.

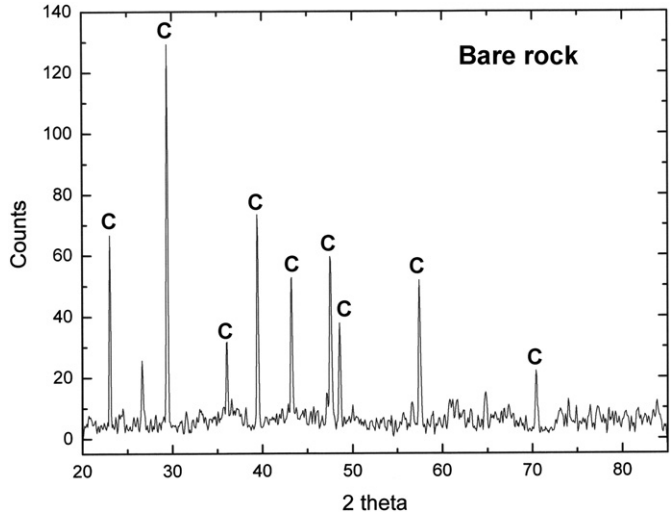

Fig. 10. Powder X-ray diffractogram of the bare rock medium. The rock is overwhelmingly calcite (calcium carbonate; $CaCO_3$), as the various peaks labeled C (calcite) indicate.

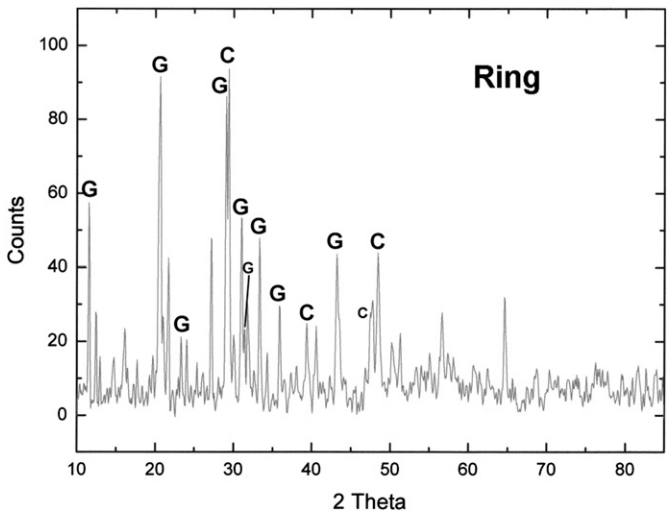

Fig. 12. Powder X-ray diffractogram of the white ring, which appears in Fig. 7. The peaks are overwhelmingly gypsum (G) with traces of calcite (C).

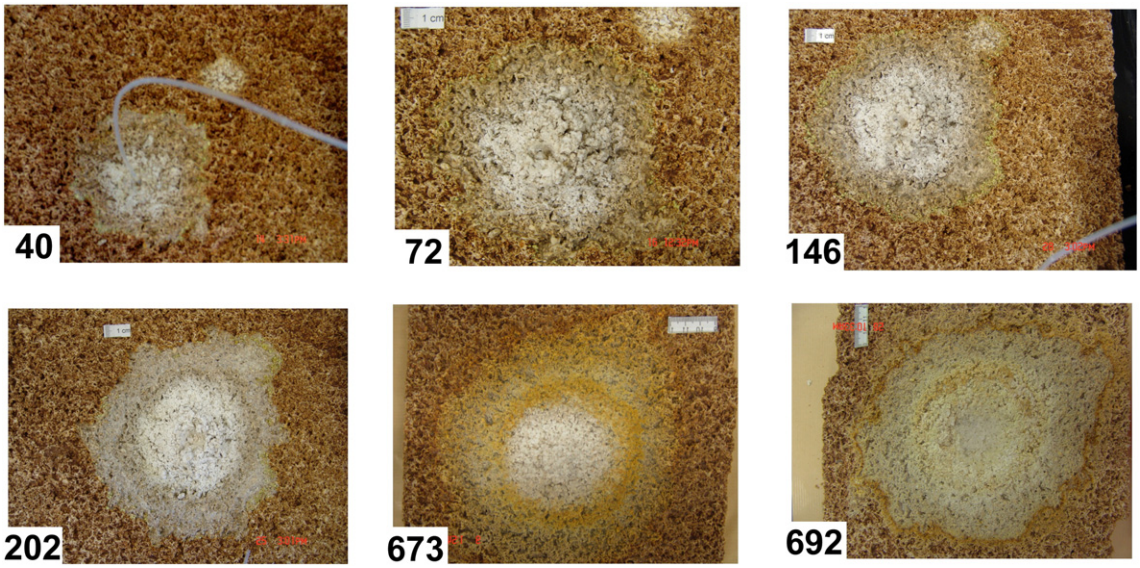

Fig. 13. Ferruginous limestone rock acidized with H_2SO_4 through the teflon tube shown. Time evolution of the rock treatment showing the gradual formation of the deposits. The numbers indicate the time in days.

domain). The % composition in gypsum (calculated for the relative mass proportions of gypsum and calcite exclusively) drops to 28.4% (see Table 3, and notably Fig. 14).

Although some gypsum is present in region 4, it has dropped significantly in favor of unreacted calcite, suggesting the residence of an interband zone, relatively depleted in the diffusing SO_4^{2-}, just as predicted by the Ostwald cycle (Ostwald, 1896–1902). Then appears a new gypsum band (region 5; 85.8% gypsum) and so on. Hence, the % composition in gypsum essentially oscillates. The complete depletion of gypsum between the bands (no 0% zones) is rendered impossible by the complex random percolation of the infiltrating acid (not a simple diffusion process), given the broad distribution of the pore sizes. The unexpectedly low composition in the last point (instead of an increase; see Fig. 14) is due to the incomplete formation of the gypsum band at that stage.

Finally, we notice a red-brown ring coloration at late stages of the pattern formation (see Fig. 13, 673 and 692 days). Because the rock has Fe^{3+} content (as shown in Sections 2.2 and 3.1 and Table 1), a reaction involving that ion must have competed with the main reactions 1 and 2. An X-ray diffractogram of the red-brown ring appearing in Fig. 13 was carried out; peaks at $2\theta = 30.0$, 36.4, 60.7 and 63.2° notably revealed the presence of Fe_2O_3.

4. Conclusions

In this paper, we simulated a Liesegang banding experiment in-situ, i.e. inside a real rock bed. After a long treatment by acid infiltration from a central source, band formation was induced in a way similar to what we see in a naturally banded rock. X-ray analysis revealed the alternation of minerals, thus resembling a 2D Liesegang pattern. A summary of the results is now presented:

1. The bare rock medium consists mainly of calcite ($CaCO_3$), with traces of monohydrocalcite ($CaCO_3 \cdot H_2O$) and $Fe_2(CO_3)_3$.
2. The deposition of $CaSO_4$ seems to appear in clear and distinct bands at an early stage of the pattern, and in regions with alternating $CaSO_4$ content after a prolonged exposure to acidization.
3. The $CaSO_4$ deposits consist essentially of the gypsum mineral ($CaSO_4 \cdot 2H_2O$), and to a lesser extent, the anhydrite mineral ($CaSO_4$, anhydrous).
4. A deposit of Fe_2O_3 indicates the presence of another reaction that competes with the main (studied) reactions within the rock medium. In a subsequent paper (Part II), we present a theoretical model to simulate the processes involved, and hence account for the band formation and alternations in the gypsum mineral. We shall also carry out a fractal analysis of the various contours of the acidization fronts.

Table 3
Variation of % gypsum over the different rock regions of Fig. 5.

Region	1	2	3	4	5	6	7
% gypsum	100	97.5	98.9	28.4	85.8	17.6	5.4

Acknowledgements

This work was supported by a grant from the Lebanese National Council for Scientific Research (LNCSR) LCR 111050.022023 (American University of Beirut; 2003–2006). The authors thank Dr. Abdel-Fattah Abdel-Rahman, for his valuable and very helpful advice. All the X-ray and AA measurements were performed in the Kamal Shair Central Research Science Lab (CRSL) of the American University of Beirut.

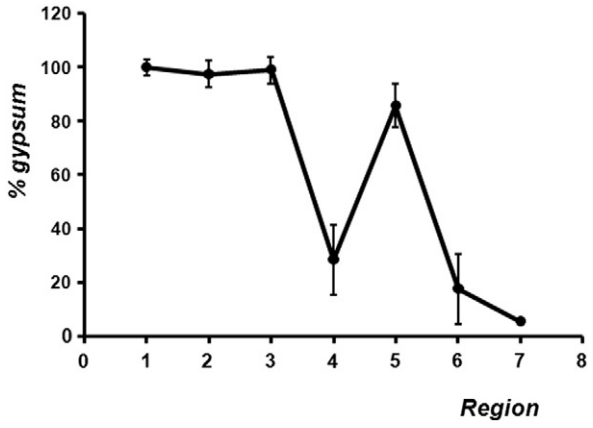

Fig. 14. Variation of the rock composition in gypsum in the various zones of Fig. 5.

References

Böhm, F., Westphal, H., Bornholdt, S., 2003. Palaeogeogr. Palaeoclimatol. Palaeoecol. 189, 161.

Boudreau, A.E., 1995. Mineral. Petrol. 54 (1–2), 55.

Boudreau, B.P., 1997. Diagenetic Models and Their Implementation: Modeling Transport and Reactions in Aquatic Sediments. Springer, Berlin.

Chacron, M., L'Heureux, I., 1999. Phys. Lett. A 263, 70–77.

Dewers, T., Ortoleva, P., 1989. J. Phys. Chem. 93, 2842 (ibid, Earth Science Reviews 29, 283 (1990)).

Fowler, A.D., L'Heureux, I., 1996. Can. Mineral. 34, 1211–1222.

Hedges, E.S., 1932. Liesegang Rings and Other Periodic Structures. Chapman and Hall, London.

Henisch, H.K., 1988. Crystals in Gels and Liesegang Rings. Cambridge University Press, Cambridge.

http://onezine.s-one.net.sg/@School/RI/garden.htm.

Jamtveit, B., Meakin, P. (Eds.), 1999. Growth, Dissolution and Pattern Formation in Geosystems. Kluwer, Dordrecht.

Klein, C., 1993. Manual of Mineralogy. 21st Ed. John Wiley and Sons, New York.

Kravchenko, V.V., Medvinskii, A.B., Reshetilov, A.N., Ivanitskii, G.R., 1999. Dokl. Akad. Nauk 364, 114 (ibid, Dokl. Akad. Nauk, 364, 687 (1999)).

Krug, H.-J., Jacob, K.-H., Dietrich, S., 1994. In: Krhul, J.H. (Ed.), in Ref, pp. 269–282.

Kruhl, J.H. (Ed.), 1994. Fractals and Dynamic Systems in Geoscience. Springer-Verlag, Berlin.

L'Heureux, I., 2013. Philos. Trans. R. Soc. A371, 20120356.

Liesegang, R.E., 1896. Chemische Fernwirkung. Lieseg. Photograph. Arch. 37, 305 (continued in 37, 331).

Liesegang, R.E., 1913. Geologische Diffusionen. In: Steinkopff, Dresden (Ed.), R. E. Liesegang, Die Achate. Steinkopf, Dresden-Leipsig, 1915.

Lifshitz, I.M., I. M., Slyozov, V.V., 1961. J. Phys. Chem. Solids 19, 35.

Lund, K., Fogler, H.S., 1976. Chem. Eng. Sci. 31, 373–380.

Lund, K., Fogler, H.S., McCune, C.C., 1973. Chem. Eng. Sci. 28, 691–700.

Merino, E., Wang, Y., 2001. In: Krug, H.-J., Kruhl, J.H. (Eds.), Year-Book for Complexity in Natural, Social, and Human SciencesNon-Equilibrium Processes and Dissipative Structures in Geoscience vol. 11. Duncker and Humblot, Berlin, pp. 13–45.

Moxon, T., 1996. Agate: Microstructure and Possible Origin. Terra Publications, Doncaster.

Moxon, T., 2001. Education in Chemistry (July) p. 105.

Msharrafieh, M., Sultan, R., 2005. ChemPhysChem 6, 2647.

Msharrafieh, M., Al-Ghoul, M., Sultan, R., 2006. In: Novak, M.M. (Ed.), Complexus Mundi: Emergent Patterns in Nature, Proceedings of the Fractals 2006 Conference, Vienna, Austria. World Scientific, Singapore, pp. 225–236.

Ohkawa, M., Yamashita, Y., Inoue, M., Itagawa, R., Takeno, S., 2000. Mineral. Petrol. 70, 15.

Ortoleva, P., 1994. Geochemical Self-Organization. Oxford University Press, New York.

Ortoleva, P., Chadam, J., Merino, E., Sen, A., 1987a. Am. J. Sci. 287, 1008–1040.

Ortoleva, P., Merino, E., Moore, C., Chadam, J., 1987b. Am. J. Sci. 287, 979–1007.

Ostwald, W., 1896–1902. Lehrbuch der Allgemeinen Chemie. 2. Aufl.2. Teil: Verwandtschaftslehre, Engelmann: Leipzig Band 2, p. 778.

Ostwald, W., 1900. Z. Phys. Chem. 34, 495.

Peng, Q., Wu, J.-G., Soloway, R.D., Hu, T.-D., Huang, W.-D., Xu, Y.-Z., Wang, L.-B., Li, X.-F., Li, W.-H., Xu, D.-F., Xu, G.-X., 1997. Biospectroscopy 3 (3), 195–205.

Ratke, L., Vorhees, P.W., 2002. Growth and Coarsening, Ostwald Ripening in Material Processing. Springer, Berlin.

Sadek, S., Sultan, R., 2011. In: Lagzi, I. (Ed.), Precipitation Patterns in Reaction-Diffusion Systems. Research Signpost publications, Trivandrum, pp. 1–43 (Chapter 1).

Shapiro, J.A., Dworkin, M. (Eds.), 1997. Bacteria as Multicellular Organisms. Oxford University Press, New York.

Sultan, R., Abdel-Rahman, A., 2013. Lat. Am. J. Solids Struct. 10, 59–73.

Sultan, R., Abdel-Rahman, A., December 5–8 2011d. Routes to pattern formation in geochemical systems. In: Awrejcewicz, J., Kaźmierczak, M., Olejnik, P., Mrozowski, J. (Eds.), Proceedings of the 11th Conference on Dynamical Systems: Theory and Applications (DSTA 2011), Łódź, Poland. Nonlinear Dynamics and Control vol. 2, pp. 471–478.

Sultan, R., Ortoleva, P., De Pasquale, F., Tartaglia, P., 1990. Earth Sci. Rev. 29, 163.

Suryanarayana, C., Grant Norton, M., 1998. X-ray diffraction, a practical approach. Experimental Module 7, Quantitative Analysis of Powder Mixtures. Plenum Press, New York, pp. 223–236.

Wang, Y., Merino, E., 1992. Geochim. Cosmochim. Acta 56, 587–596.

Wang, Y., Chan, M.A., Merino, E., 2015. Sci. Rep. 5, 10792.

Xie, D., Wu, J., Xu, G., Ouyang, Q., Soloway, R.D., Hu, T., 1999. J. Phys. Chem. B 103, 8602–8605.

Zaknoun, F., El-Rassi, H., Al-Ghoul, M., Al-Joubeily, S., Mokalled, T., Sultan, R., 2010. In: Skiadas, C.H., Dimotikalis, I. (Eds.), Chaotic Systems: Theory and Applications. World Scientific, pp. 385–394.